J|A|C|S
ARTICLES
Published on Web 12/20/2006

High-Resolution Electronic Spectra of Ethylenedioxythiophene Oligomers

Dorothee Wasserberg,[†] Stefan C. J. Meskers,[†] René A. J. Janssen,*[,†] Elena Mena-Osteritz,[‡] and Peter Bäuerle*[,‡]

Contribution from Molecular Materials and Nanosystems, Eindhoven University of Technology, P.O. Box 513, NL-5600 MB Eindhoven, The Netherlands, and Institute of Organic Chemistry II, University of Ulm, Albert-Einstein-Allee 11, D-89081 Ulm, Germany

Received September 26, 2006; E-mail: r.a.j.janssen@tue.nl; peter.baeuerle@uni-ulm.de

Abstract: The photophysical properties of a series of 3,4-ethylenedioxythiophene oligomers (OEDOT) with up to five repeat units are studied as function of conjugation length using absorption, fluorescence, phosphorescence, and triplet−triplet absorption spectroscopy at low temperature in a rigid matrix. At 80 K, a remarkably highly resolved vibrational fine structure can be observed in the all electronic spectra which reveals that the electronic structure of the oligomers strongly couples to two different vibrational modes (∼180 and ∼50 meV). The energies of the 0−0 transitions in absorption, and fluorescence, phosphorescence, and triplet−triplet absorption all show a reciprocal dependence on the inverse number of repeat units. The triplet energies inferred from the phosphorescence spectra are accurately reproduced by quantum chemical DFT calculations using optimized geometries for the singlet ground state (S_0) and first excited triplet state (T_1). Using vibrational IR and Raman spectroscopy and quantum chemical DFT calculations for the normal modes in the ground state, we have been able to assign the vibrations that couple to the electronic structure to fully symmetric normal modes. The high-energy mode is associated with the well-known carbon−carbon bond stretch vibration, and the low-energy mode involves a deformation of the bond angles within the thiophene rings and a change of C−S bond lengths. Experimentally obtained Huang−Rhys parameters and theoretical normal mode deformations are used to analyze the geometry changes between T_1 and S_0 and to semiexperimentally predict the geometry in the S_1 state for 2EDOT.

Introduction

Poly(3,4-ethylenedioxythiophene) (PEDOT) is one of the most successful conducting polymers. It combines a high conductivity in the oxidized state with good stability under ambient conditions. The high stability in the doped state originates from the electron donating ethylenedioxy substituents that lower the oxidation potential. Because of these beneficial properties PEDOT is commonly used in antistatic applications, as electrode material in solid electrolyte capacitors, polymer light-emitting diodes, and photovoltaic cells, and for electrochromic windows and displays.[1,2] In recent years the EDOT unit has also been used in combination with other functional moieties to achieve redox active systems.[3−8] By modifying the bridge into an enantiomerically pure chiral moiety a stereoregular and regioregular PEDOT derivative has been designed. The chirality in the derivatized ethylenedioxy bridge has been shown to influence the photo- and spectroelectrical properties of the compound.[9,10]

In the same way as the case for many other conjugated polymers, detailed knowledge on the electrical, optical, and electrochemical properties of PEDOT has been obtained by studying well-defined oligomers with different conjugation lengths.[11] The first OEDOTs to be synthesized were the dimer and trimer (2EDOT and 3EDOT);[12−15] 3EDOT was described as being highly unstable.[13] To increase chemical stability and to preserve monodispersity, a variety of α,α′ end-capped oligomers employing mesitylthio,[16] phenyl,[17,18] and hexyl[19]

[†] Eindhoven University of Technology.
[‡] University of Ulm.

(1) Groenendaal, L.; Jonas, F.; Freitag, D.; Pielartzik, H.; Reynolds, J. R *Adv. Mater.* **2000**, *12*, 481−494.
(2) Groenendaal, L.; Zotti, G.; Aubert, P. H.; Waybright, S. M.; Reynolds, J. R. *Adv. Mater.* **2003**, *15*, 855−879.
(3) Argun, A. A.; Cirpan, A.; Reynolds, J. R. *Adv. Mater.* **2003**, *15*, 1338−1341.
(4) Argun, A. A.; Aubert, P. H.; Thompson, B. C.; Schwendeman, I.; Gaupp, C. L.; Hwang, J.; Pinto, N. J.; Tanner, D. B.; MacDiarmid, A. G.; Reynolds, J. R. *Chem. Mater.* **2004**, *16*, 4401−4412.
(5) Thomas, C. A.; Zong, K.; Abboud, K. A.; Steel, P. J.; Reynolds, J. R. *J. Am. Chem. Soc.* **2004**, *126*, 16440−16450.
(6) Huchet, L.; Akoudad, S.; Levillain, E.; Roncali, J.; Emge, A.; Bäuerle, P. *J. Phys. Chem. B* **1998**, *102*, 7776−7781.
(7) Segura, J. L.; Gomez, R.; Reinold, E.; Bäuerle, P. *Org. Lett.* **2005**, *7*, 2345−2348.
(8) Segura, J. L.; Gomez, R.; Blanco, R.; Reinold, E.; Bäuerle, P. *Chem. Mater.* **2006**, *18*, 2834−2847.
(9) Caras-Quintero, D.; Bäuerle, P. *Chem. Commun.* **2002**, 2690−2691.
(10) Caras-Quintero, D.; Bäuerle, P. *Chem. Commun.* **2004**, 926−927.
(11) Wegner, G., Müllen, K., Eds. *Electronic Materials: The Oligomer Approach*; Wiley-VCH: Weinheim, 1996.
(12) Sotzing, G. A.; Reynolds, J. R.; Steel, P. J. *Chem. Mater.* **1996**, *8*, 882−889.
(13) Sotzing, G. A.; Reynolds, J. R.; Steel, P. J. *Adv. Mater.* **1997**, *9*, 795−798.
(14) Akoudad, S.; Roncali, J. *Synth. Met.* **1998**, *93*, 111−114.
(15) Zhu, S. S.; Swager, T. M. *J. Am. Chem. Soc.* **1997**, *119*, 12568−12577.
(16) Hicks, R. G.; Nodwell, M. B. *J. Am. Chem. Soc.* **2000**, *122*, 6746−6753.
(17) Apperloo, J. J.; Groenendaal, L. B.; Verheyen, H.; Jayakannan, M.; Janssen, R. A. J.; Dkhissi, A.; Beljonne, D.; Lazzaroni, R.; Brédas, J. L. *Chem.−Eur. J.* **2002**, *8*, 2384−2396.

groups were prepared and studied in detail using cyclic voltammetry, optical absorption, and electron spin resonance. The synthesis and properties of OEDOTs have been reviewed by Groenendaal et al.[1,2] and Roncali et al.[20] and remain a topical field of experimental[21−27] and theoretical research.[28,29] Recently, OEDOTs have also been used for their semiconducting properties in field-effect transistors[30] and in organic photovoltaic diodes.[31]

Systematic photophysical studies on a series of π-conjugated oligomers have been reported for oligophenylene vinylenes,[32−36] oligofluorenes,[37−40] and abundantly for oligothiophenes.[41] For a series of phenyl end-capped OEDOTs, fluorescence and phosphorescence at low temperature have been described recently;[22] however, in general the photophyiscal properties of OEDOTs have received surprisingly little attention. Here a comprehensive study of the electronic and vibrational spectra of a novel series of trimethylsilyl end-capped OEDOTs (*n*EDOT−TMS_2) with *n* up to five EDOT units will be presented (Figure 1).[42] For comparison purposes 2EDOT and 3EDOT have been synthesized from the corresponding 2- and 3EDOT−TMS_2[42] and were both found to be astonishingly stable, contrary to published results.[13] The UV/vis absorption, fluorescence, phosphorescence, and transient absorption, as well as Raman and infrared spectra, of these compounds have been studied to determine the nature of the first excited singlet (S_1) and triplet (T_1) states and to compare these experiments with density functional theory (DFT) calculations. It will be shown that, in a rigid matrix at low temperature, the absorption and photoluminescence spectra of the OEDOTs exhibit an extremely well resolved vibrational fine structure due to coupling with two different vibrational modes. Based on the spectra and DFT calculations, the vibrational frequencies are assigned to specific normal modes, which allowed a semiexperimental estimate of the geometry in the singlet excited state to be made.

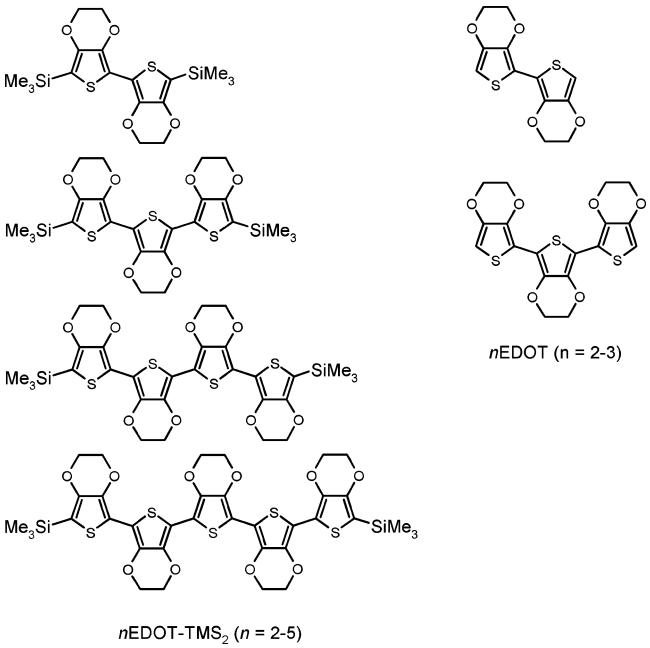

Figure 1. Ethylenedioxythiophene oligomers *n*EDOT and *n*EDOT−TMS_2 used in this study.

Results and Discussions

Absorption and Fluorescence at Room Temperature. The normalized absorption and fluorescence spectra of the OEDOTs measured in dichloromethane at room temperature show a broad spectrum with a partially resolved vibrational progression (Figure 2). The appearance of a vibrational fine structure in the absorption spectrum at room temperature in solution is a fairly unique property of OEDOTs and is generally not observed for unsubstituted or alkyl substituted oligothiophenes.[41] The broad structureless absorption band that is commonly observed for oligothiophenes is due to inhomogeneous broadening which results from the fact that the spectra of the individual molecules in solution are slightly different because of conformational (rotational) disorder. This often obscures the vibrational structure in the electronic spectra and leads to broad structureless bands. The explanation for the exceptional resolution in the room-temperature spectra of the OEDOTs is likely the attractive interaction that exists between the sulfur and oxygen atoms in a transoid conformation. A crystallographic study of 2EDOT has revealed that the distance between oxygen and sulfur atoms of adjacent units is only 2.92 Å and hence significantly shorter than the sum of the van der Waals radii of sulfur and oxygen (3.25 Å), giving evidence of the occurrence of strong intramolecular interactions.[43] It can be presumed that the attractive O···S interactions of alternating monomers stabilize a transoid conformation of the rings and a fully planar structure of the oligomer that is more resistant to inter-ring rotations than

(18) De Jong, M. P.; Denier, van der Gon, A. W.; Crispin, X.; Osikowicz, W.; Salaneck, W. R.; Groenendaal, L. *J. Chem. Phys.* **2003**, *118*, 6495−6502.
(19) Turbiez, M.; Frère, P.; Roncali. *J. Org. Chem.* **2003**, *68*, 5357−5360.
(20) Roncali, J.; Blanchard, P.; Frère, P. *J. Mater. Chem.* **2005**, *15*, 1589−1610.
(21) Turbiez, M.; Frère, P.; Roncali, J. *Tetrahedron.* **2005**, *61*, 3045−3053.
(22) Wasserberg, D.; Marsal, P.; Meskers, S. C. J.; Janssen, R. A. J.; Beljonne, D. *J. Phys. Chem. B* **2005**, *109*, 4410−4415.
(23) Turbiez, M.; Frère, P.; Allain, M.; Gallego-Planas, N.; Roncali, J. *Macromolecules* **2005**, *38*, 6806−6812.
(24) Casado, J.; Ponce Ortiz, R.; Ruiz Delgado, M. C.; Hernández, V.; López Navarrete, J. T.; Raimundo, J. M.; Blanchard, P.; Allain, M.; Roncali, J. *J. Phys. Chem. B* **2005**, *109*, 16616−16627.
(25) Jousselme, B.; Blanchard, P.; Allain, M.; Levillain, E.; Dias, M.; Roncali, J. *J. Phys. Chem. A* **2006**, *110*, 3488−3494.
(26) Leriche, P.; Blanchard, P.; Frère, P.; Levillain, E.; Mabon, G.; Roncali, J. *Chem. Commun.* **2006**, 275−277.
(27) Perepichka, I. F.; Roquet, S.; Leriche, P.; Raimundo, J. M.; Frère, P.; Roncali, J. *Chem.−Eur. J.* **2006**, *12*, 2960−2966.
(28) Dkhissi, A.; Beljonne, D.; Lazzaroni, R.; Louwet, F.; Groenendaal, L.; Brédas, J. L. *Int. J. Quantum Chem.* **2003**, *91*, 517−523.
(29) Alemán, C.; Armelin, E.; Iribarren, J. I.; Liesa, F.; Laso, M.; Casanovas, J. *Synth. Met.* **2005**, *149*, 151−156.
(30) Turbiez, M.; Frère, P.; Allain, M.; Videlot, C.; Ackermann, J.; Roncali, J. *Chem.−Eur. J.* **2005**, *11*, 3742−3752.
(31) Roncali, J.; Frère, P.; Blanchard, P.; de Bettignes, R.; Turbiez, M.; Roquet, S.; Leriche, P.; Nicolas, Y. *Thin Solid Films* **2006**, *511−512*, 567−575.
(32) Schenk, R.; Gregorius, H.; Meerholz, K.; Heinze, J.; Müllen, K. *J. Am. Chem. Soc.* **1991**, *113*, 2634−2647.
(33) Oelkrug, D.; Tompert, A.; Egelhaaf, H. J.; Hannack, M.; Steinhuber, E.; Hohloch, M.; Meier, H.; Stalmach, U. *Synth. Met.* **1996**, *83*, 231−237.
(34) Cornil, J.; Beljonne, D.; Heller, C. M.; Campbell, I. H.; Laurich, B. K.; Smith, D. L.; Bradley, D. D. C.; Müllen, K.; Brédas, J. L. *Chem. Phys. Lett.* **1997**, *278*, 139−145.
(35) Peeters, E.; Ramos, A. M.; Meskers, S. C. J.; Janssen, R. A. J. *J. Chem. Phys.* **2000**, *112*, 9445−9454.
(36) Gierschner, J.; Mack, H. G.; Lüer, L.; Oelkrug, D. *J. Chem. Phys.* **2002**, *116*, 8596−8609.
(37) Klaerner, G.; Miller, R. D. *Macromolecules* **1998**, *31*, 2007−2009.
(38) Jo, J.; Chi, C.; Höger, S.; Wegner, G.; Yoon, D. Y. *Chem.−Eur. J.* **2004**, *10*, 2681−2688.
(39) Yasuda, T.; Fujita, K.; Tsutsui, T.; Geng, Y.; Culligan, S. W.; Chen, S. H. *Chem. Mater.* **2005**, *17*, 264−268.
(40) Wasserberg, D.; Dudek, S. P.; Meskers, S. C. J.; Janssen, R. A. J. *Chem. Phys. Lett.* **2005**, *411*, 273−277.
(41) Fichou, D., Ed. *Handbook of Oligo- and Polythiophenes*; Wiley-VCH: Weinheim, 1999.
(42) Reinold, E.; Nicklas, F.; Vogt, A.; Bäuerle, P. In preparation.
(43) Raimundo, J. M.; Blanchard, P.; Frère, P.; Mercier, N.; Ledoux-Rak, I.; Hierle, R.; Roncali, J. *Tetrahedron Lett.* **2001**, *42*, 1507−1510.

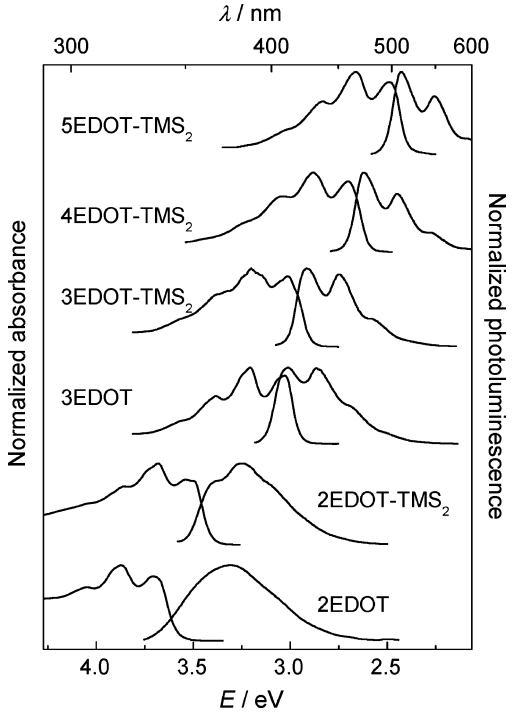

Figure 2. Normalized UV/vis (O.D. ≈ 1) and fluorescence (O.D. ≈ 0.1) spectra of the OEDOTs in dichloromethane recorded at room temperature. For clarity the spectra are offset vertically.

Table 1. Peaks of Lowest Energy Absorption (E^{abs}), Highest Energy Emission (E^{em}), and Their Difference (Δ) for OEDOTs in Solution, the Fluorescence Quantum Yield (ϕ), Lifetime (τ), Radiative Lifetimes from Experiment (τ/ϕ) and from the Strickler−Berg Equation (τ_{rad}), and the Triplet State Lifetime ($\tau(T_1)$)

compound	E^{abs} (eV)	E^{em} (eV)	Δ (eV)	φ	τ^a (ns)	τ/ϕ (ns)	$\tau_{rad}{}^b$ (ns)	$\tau\ (T_1)^c$ (μs)
2EDOT	3.71							
2EDOT−TMS_2	3.54	3.39	0.15	0.01				2500
3EDOT	3.03	3.01	0.02	0.06	0.097	1.6	2.84	230
3EDOT−TMS_2	3.01	2.92	0.09	0.08	0.144	1.8	2.55	450
4EDOT−TMS_2	2.71	2.62	0.09	0.17	0.259	1.5	2.37	148
5EDOT−TMS_2	2.49	2.43	0.06	0.24	0.586	2.4	2.38	83[d]

[a] Measured in dichloromethane. [b] Determined using the Strickler−Berg equation. [c] From time-dependent phosphorescence spectra at 80 K. [d] From triplet PIA spectra at 80 K.

oligothiophenes that lack the ethylenedioxy bridge. As a consequence of the more rigid molecular structure in solution, the inhomogeneous broadening is reduced and structured absorption spectra are observed for all OEDOTs in solution. The fluorescence spectra are also structured for *n*EDOTs and *n*EDOT−TMS_2s with $n > 2$ and a small shift is observed between the corresponding first peaks in absorption and emission. Although 2EDOT and 2EDOT−TMS_2 present structured absorption spectra, the fluorescence spectra are less structured than the higher homologues. As expected, the 0−0 transitions of the absorption and fluorescence spectra shift to lower energy with increasing oligomer length.

The fluorescence lifetime (see Supporting Information) measured for the longer ($n > 2$)[44] OEDOTs in dichloromethane increases with increasing chain length from $\tau = 97$ ps for 3EDOT to 586 ps for 5EDOT−TMS_2 (Table 1). The fluorescence quantum yield (ϕ) of the oligomers also increases with chain length, and as a consequence the radiative lifetimes τ/ϕ differ only slightly in the OEDOT series (Table 1).

(44) The excitation wavelength (400 nm) of the picosecond laser used in these experiments could not be used to excite H-2EDOT and TMS-2EDOT.

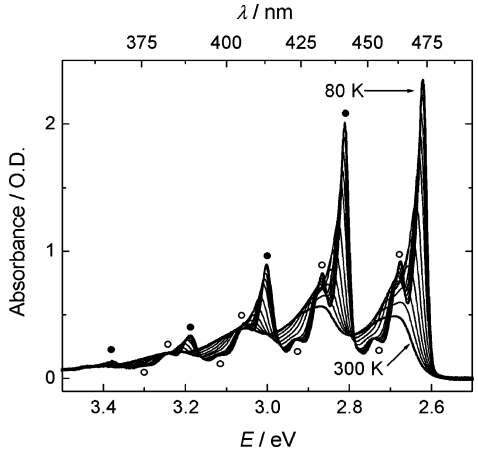

Figure 3. UV/vis absorption spectra of 4EDOT−TMS_2 in MeTHF upon cooling from 300 to 80 K. Solid and open circles label the vibronic replicas of the main 0−0 transition (see text).

The radiative lifetimes associated with the singlet state of the OEDOTs can also be estimated from the experimental absorption and fluorescence spectra using the Strickler−Berg equation for a nondegenerate excited state:[45]

$$\frac{1}{\tau_{rad}} = 2.880 \times 10^9 n^2 \langle \tilde{\nu}_f^{-3} \rangle_{av}^{-1} \int \epsilon \, d \ln \tilde{\nu} \qquad (1)$$

$$\langle \tilde{\nu}_f^{-3} \rangle_{av}^{-1} = \frac{\int I(\tilde{\nu}) \, d\tilde{\nu}}{\int \nu^{-3} I(\tilde{\nu}) \, d\tilde{\nu}} \qquad (2)$$

in which n is the refractive index of the solvent, ϵ, the molar absorption coefficient, and I, the intensity of the fluorescence spectrum. The radiative lifetimes (τ_{rad}) estimated with the Strickler−Berg equation are collected in Table 1. Their magnitudes are in fair agreement with the experimental τ/ϕ values, which we ascribe to the limited accuracy in determining ϕ and the integral molar absorption coefficient. Despite the fact that the trends do not agree, the calculated values confirm the experimental result that the radiative lifetime does not vary strongly with the conjugation length of the oligomer.

Absorption and Fluorescence at Low Temperature. The partially resolved vibronic structure in the UV/vis absorption of the OEDOTs observed at room temperature undergoes major transformations when lowering the temperature. As an example, the changes in the absorption spectrum of 4EDOT−TMS_2 in MeTHF solution with decreasing temperature are shown in Figure 3. Upon decreasing the temperature, the vibronic peaks sharpen and become more intense. At low temperatures, the spectra clearly show two different vibrational progressions with different energy splittings. For the highest energy splitting up to four replicas can be found at higher energies (Figure 4, solid circles), while two additional peaks are observed for the low-energy progression (Figure 4 open circles). At low temperatures the 0−0 transition of both vibrational progressions has the highest intensity. Despite the major changes in the spectra, the onset of the spectrum remains unchanged with respect to the room-temperature spectra. The changes with temperature are

(45) Strickler, S. J.; Berg, R. A. *J. Chem. Phys.* **1962**, *37*, 814−822.

Table 2. Experimental 0−0 Transition Energies (E_{00}) in Absorption, Fluorescence, Phosphorescence, and Triplet Absorption, the Vibrational Spacing ($\tilde{\nu}_1$,$\tilde{\nu}_2$), Line Widths Γ, and Huang−Rhys Parameters (S_1, S_2) of the OEDOTS, and the Theoretical Triplet State Energies (E_{DFT}) from DFT Calculations

	absorption $S_1 \leftarrow S_0$						fluorescence $S_1 \rightarrow S_0$					
compound	E_{00} (eV)	$\tilde{\nu}_1$ (meV)	$\tilde{\nu}_2$ (meV)	Γ (meV)	S_1	S_2	E_{00} (eV)	$\tilde{\nu}_1$ (meV)	$\tilde{\nu}_2$ (meV)	Γ (meV)	S_1	S_2
2EDOT	3.66	195	57	15	0.92	0.72	3.65	185	59	25	1.05	0.75
2EDOT−TMS_2	3.47	195	57	16	0.90	0.59	3.46	183	57	28	1.08	0.60
3EDOT	3.05	194	56	14	0.89	0.52	3.04	180	51	20	0.98	0.45
3EDOT−TMS_2	2.93	194	55	13	0.86	0.45	2.93	183	55	25	0.78	0.40
4EDOT−TMS_2	2.62	190	54	14	0.86	0.39	2.61	180	53	18	0.83	0.39
5EDOT−TMS_2	2.42	188	54	17	0.80	0.30	2.41	182	49	15	0.68	0.32

	phosphorescence $T_1 \rightarrow S_0$							triplet absorption $T_n \leftarrow T_1$				
compound	E_{00} (eV)	E_{DFT} (eV)	$\tilde{\nu}_1$ (meV)	$\tilde{\nu}_2$ (meV)	Γ (meV)	S_1	S_2	E_{00} (eV)	$\tilde{\nu}_1$ (meV)	$\tilde{\nu}_2$ (meV)	Γ (meV)	S_1
2EDOT	2.18	2.09	178	64	38	1.12	1.03					
2EDOT−TMS_2	2.13	2.01	175	59	28	1.79	0.88	2.80	158			0.36
3EDOT	1.79	1.67	181	60	25	0.74	0.65	2.50	179			0.36
3EDOT−TMS_2	1.76	1.63	180	55	25	0.68	0.55	2.39	185			0.35
4EDOT−TMS_2	1.57	1.44		63				2.04	174			0.38
5EDOT−TMS_2	1.45	1.33						1.84	196	74	16	0.20[a]

[a] For 5EDOT−TMS_2 the S_2 parameter is 0.10.

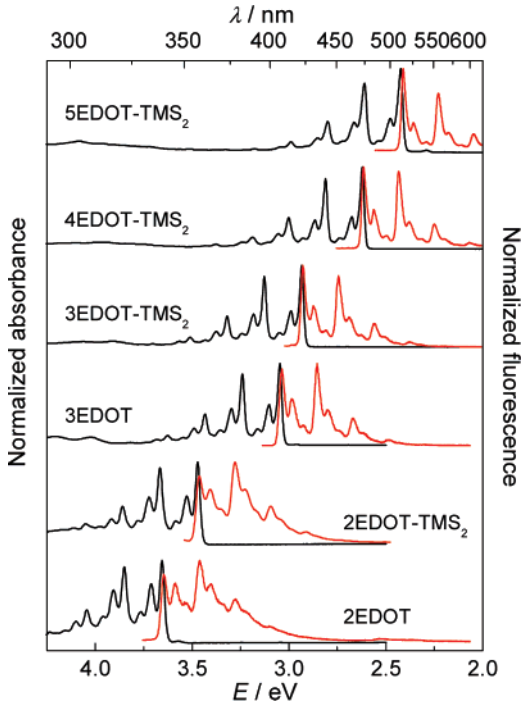

Figure 4. Normalized UV/vis (O.D. ≈ 1) and fluorescence (O.D. ≈ 0.1) spectra of OEDOTs in frozen MeTHF recorded at 80 K. For clarity the spectra are offset vertically.

interpreted as a continuous loss of the remaining conformational disorder, and it is assumed that at lower temperature the oligomers become more planar and more similar in their conformation with an all-transoid configuration of the thiophene rings. This reduces the inhomogeneous broadening and leads to the highly resolved spectra of 4EDOT−TMS_2 (Figure 4). To the best of our knowledge, the resolution of two different progressions has not been observed before in similar detail in the electronic absorption spectra of conjugated oligomers in a condensed phase at 80 K.

Similar changes occur for all other OEDOTs. Their absorption spectra recorded at 80 K in MeTHF are collected in Figure 4. For each oligomer, two distinct vibronic progressions are observed, corresponding to vibrational modes with energies of $\tilde{\nu}_1 \approx 180$ meV (∼1450 cm^{-1}) and $\tilde{\nu}_2 \approx 56$ meV (∼450 cm^{-1}). The 0−0 transition has the highest intensity for each of the OEDOTs and becomes more pronounced for the longer oligomers. Furthermore, a clear shift of the 0−0 transition to lower energy with increasing length is observed.

The change in temperature also has a strong effect on the fluorescence of the OEDOTs. The fluorescence spectra recorded in MeTHF at 80 K also exhibit two well-resolved vibronic progressions with a similar energy splitting as the ones in the absorption. At low temperature the fluorescence spectra are near perfect mirror images of the absorption spectra.

Under these low-temperature conditions in MeTHF, the Stokes shift is extremely small (≤0.01 eV). The small Stokes shift is consistent with the molecules being confined to rigid cavities in the frozen solvent at low temperatures (80 K), eliminating the solvent relaxation that causes a Stokes shift. The relative intensities of the vibrational peaks in the fluorescence change with the length of the oligomer. This issue will be discussed in more detail later on in relation to the geometry relaxation in the excited state. The energies of the 0−0 transitions, E_{00}, are listed in Table 2 for all oligomers together with the vibrational energies ($\tilde{\nu}_1$,$\tilde{\nu}_2$) of the two progressions. Highly resolved fluorescence spectra for oligothiophenes have previously been observed for bithiophene, terthiophene, and quaterthiophene in *n*-alkanes at 4.2 K,[46−49] but for these oligomers the $\tilde{\nu}_2 \approx 450$ cm^{-1} progression was not observed.

When plotting E_{00} versus the reciprocal number of repeat units of the oligomer, an approximately linear relation is found (Figure 5). The energy of the high-energy vibrational mode ($\tilde{\nu}_1$) in the absorption spectrum is slightly higher (6−14 meV) than that of the same mode in the fluorescence spectra, while the low-energy modes ($\tilde{\nu}_2$) have frequencies that are virtually identical. This leads to the conclusion that the potential energy diagrams

(46) Birnbaum, D.; Kohler, B. E. *J. Chem. Phys.* **1991**, *95*, 4783−4789.
(47) Birnbaum, D.; Kohler, B. E. *J. Chem. Phys.* **1989**, *90*, 3506−3510.
(48) Birnbaum, D.; Fichou, D.; Kohler, B. E. *J. Chem. Phys.* **1992**, *96*, 165−169.
(49) Gierschner, J.; Mack, H. G.; Egelhaaf, H. J.; Schweizer, S.; Doser, B.; Oelkrug, D. *Synth. Met.* **2003**, *138*, 311−315.

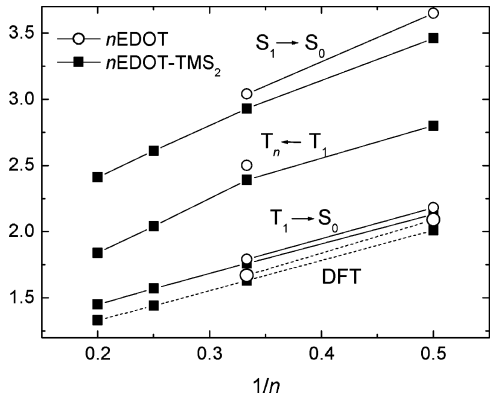

Figure 5. Energies of the E_{00} transitions of *n*EDOTs (○) and *n*EDOT−TMS_2s (■) observed in fluorescence ($S_1 \rightarrow S_0$), phosphorescence ($T_1 \rightarrow S_0$), triplet absorption ($T_n \leftarrow T_1$), and the triplet state energy from DFT calculations (DFT) as function of the reciprocal number of repeat units (*n*) in the oligomer.

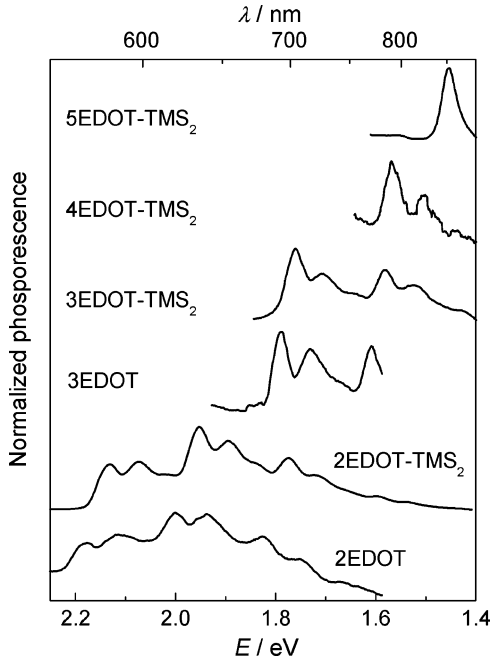

Figure 6. Phosphorescence spectra of OEDOTs in frozen MeTHF recorded at 80 K. For clarity the spectra are offset vertically.

and force constants of the ground state (S_0) and the first excited singlet state (S_1) are very similar for both modes, but that the potential energy curve of the S_0 state is slightly broader along the high-energy mode than that in the S_1 state.

Within one series of oligomers, the vibrational frequencies are almost constant for different lengths. From 2EDOT−TMS_2 to 5EDOT−TMS_2 the high-frequency mode shows a small decrease from 195 to 188 meV, while this mode exhibits no obvious trend with length in the fluorescence spectra. Also the variations in the frequency of the lower energy mode are minor.

Phosphorescence at Low Temperature. The phosphorescence spectra of the OEDOTs (Figure 6) were recorded at 80 K in frozen MeTHF using pulsed (4 ns) laser excitation and time-gated detection, starting 100 ns after the laser pulse to avoid contamination of the low-intensity phosphorescent signal with the more intense short-lived fluorescence. The spectral features appear at distinctly (∼1 eV) lower energies than the fluorescence and show a clear 0−0 transition accompanied with a vibronic fine structure at lower energies. The energy spacing in the fine

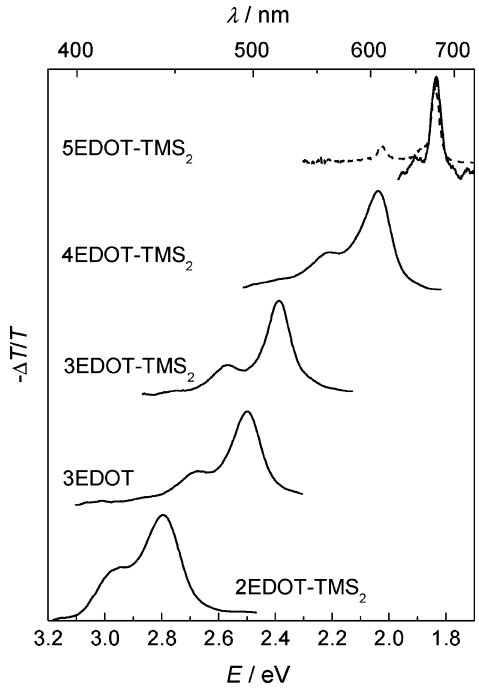

Figure 7. Normalized transient photoinduced absorption spectra ($-\Delta T/T$) of the OEDOTs in frozen MeTHF (O.D. ≈ 1) recorded at 80 K. For 5EDOT−TMS_2 spectra recorded by transient (solid line) and near steady state (dashed line) setups are shown. For details concerning the two setups see the Supporting Information. The spectra are offset vertically for clarity.

structure of the phosphorescence spectra is similar to that observed in absorption and fluorescence. The lifetime of the phosphorescence $\tau(T_1)$ was found to be in the microsecond to millisecond regime, ranging from 83 μs for 5EDOT−TMS_2 up to 2.5 ms for 2EDOT−TMS_2 (Table 1). The large red shift, the vibrationally resolved emission, and the long lifetimes are all consistent with the phosphorescence ($T_1 \rightarrow S_0$) originating form the first-excited triplet state of the OEDOTs.

The triplet state energy that can be obtained from the 0−0 transition in the spectra (Table 2) decreases almost linearly with the inverse oligomer length from 2.13 to 1.45 eV for 2EDOT−TMS_2 to 5EDOT−TMS_2 (Figure 5). The slope of a linear fit of the energy with the reciprocal number is smaller for the $T_1 \rightarrow S_0$ transition than for the $S_1 \rightarrow S_0$ transition. This suggests that the T_1 state is less delocalized than the S_1 state.

As mentioned, the phosphorescence spectra show two distinct coupling modes. The high-frequency mode (175−180 meV) (Table 2) could only be measured for the shorter oligomers ($n = 2$ and 3) because the vibronic features of the longer oligomers ($n = 4$ and 5) were outside the detection range (<850 nm). The energy of the low-frequency mode (55−64 meV) could be estimated for all oligomers except 5EDOT−TMS_2. There is little variation among these values for the different molecules, and there is no clear dependence on the length of the oligomer.

Triplet−Triplet Absorption at Low Temperature. Transient photoinduced absorption (PIA) spectra of the OEDOTs in frozen MeTHF were recorded using pulsed (4 ns) laser excitation and gated detection of a continuous white probe light at 80 K (Figure 7). The PIA spectra show a strong band that can be associated with the $T_n \leftarrow T_1$ transition of the triplet state. The 0−0 transitions can be clearly discerned at the red edge in the PIA spectra, and the position decreases with increasing oligomer length from 2EDOT−TMS_2 at 2.80 eV to 5EDOT−

TMS_2 at 1.84 eV. The energy of the $T_n \leftarrow T_1$ transition shows a reciprocal dependence on the number of repeat units as displayed in Figure 5.

Some of vibrational fine structure is apparent in the triplet absorption spectra, although less resolved than observed in the linear absorption and emission spectra. Consequently, only the high-energy vibrational splitting (~170 meV, Table 2) can be seen. The second, low-energy mode is only discernible for 5EDOT−TMS_2 and is about 70 meV. The energies of these two modes are similar to those found for ground state and singlet excited state, suggesting that in all cases similar vibrational modes couple to the electronic transitions.

Vibrational Spectroscopy. In the previous sections it was shown that at 80 K in frozen MeTHF each of the OEDOTs show $S_1 \leftarrow S_0$, $S_1 \rightarrow S_0$, $T_1 \rightarrow S_0$, and $T_n \leftarrow T_1$ transitions exhibiting a vibrational fine structure indicating coupling of these electronic transitions to two vibrational modes. The energies associated with these modes are similar in each of the spectra. In this section, the vibrational fine structure will be analyzed in more detail and compared to vibrational spectra recorded with FT−IR and FT−Raman.

The discussion will be focused on the fine structure in the fluorescence spectra because these are highly resolved and the vibrational modes in fluorescence correspond to the potential energy diagram of the ground state (S_0) and can thus be compared to IR and Raman spectroscopy. The average vibration energies, including the deviations, of the different EDOT oligomers for the two modes are 182 ± 3 meV (1470 ± 20 cm^{-1}) and 54 ± 5 meV (435 ± 40 cm^{-1}) (Table 2). The 1470 cm^{-1} mode has been observed in many different types of π-conjugated systems and is generally assigned to a symmetric C═C stretching mode. The low-energy mode has an energy that places it in the regime of deformational/torsional modes.

To study the vibrations in more detail, the FT−Raman and FT−IR spectra of the OEDOTs were recorded. For FT−IR, the oligomers were dispersed in KBr pellets, while FT-Raman spectra were obtained with a 1064 nm excitation on powdered samples. The vibrational spectra were recorded at room temperature and are shown in Figures 8 and 9 for the high- and low-energy regimes, respectively. Qualitatively, most of the features in the vibrational spectra are consistent with those previously observed for α,α′-end-capped oligothiophenes.[50−56]

In the high wavenumber region (Figure 8), the FT−IR spectra show three vibrations at approximately 1360, 1430, and 1462 cm^{-1}. Their positions are almost invariant with the length of the oligomer, but for 2EDOT and 3EDOT the last two modes appear at slightly (6−9 cm^{-1}) higher wavenumbers. The FT−Raman spectra are more complex and exhibit bands whose positions and shapes shift more strongly with oligomer length and nature of the end group. For the two transitions at ~1437 and ~1455 cm^{-1}, the positions are (in first approximation) fairly constant among the different OEDOTs. Two other transitions, at higher energies (1478−1512 cm^{-1} and 1549−1598 cm^{-1}) clearly show more dispersion.

The FT−IR spectra show a large number of transitions in the low wavenumber region (Figure 9). In the region of interest (400−500 cm^{-1}), the FT−IR spectra show a strong band at 451 cm^{-1} for the TMS-functionalized oligomers but not for the hydrogen terminated derivatives that show a transition at 410 cm^{-1}. Two additional bands associated with the TMS groups are at 630 and 755 cm^{-1}. In contrast, the Raman spectra do show a distinct band at ~440 cm^{-1} that is close to low-energy progression observed in the fluorescence spectra of both types of OEDOTs.

DFT Calculations. Quantum chemical calculations can provide additional information on the OEDOTs. Density functional theory (DFT) has been used to describe the geometric and electronic structures in the S_0 singlet ground state and T_1 triplet excited state. A potential including both Becke and Hartree−Fock exchange and Lee, Yang, and Parr correlation (B3LYP) and a split-valence 6-31G* basis set have been used to optimize the S_0 and T_1 geometries of all OEDOTs.[57]

When using optimized S_0 and T_1 geometries, the energy of the T_1 state corresponds to the energy difference between the minima of the potential energy surfaces, while the experimental 0−0 transition corresponds to the difference between the zero-point energies (ZPEs) of the two states. Since the dominant vibrational modes and frequencies are similar for the singlet and triplet manifold, the error introduced by neglecting the vibrational effects is likely to be smaller than the observed differences. The T_1-S_0 energies obtained from the DFT calculations (Table 2) are in excellent agreement with the experimental values from the phosphorescence spectra (subject to a systematic deviation of ~0.12 eV) and reproduce the experimental chain length dependence accurately (Figure 5).[22]

The optimized geometries are very similar for all OEDOTs in both electronic states. All thiophene rings, including the two oxygen atoms, are essentially coplanar within a <1° accuracy. The ethylenedioxy bridges have dihedral angles (O−C−C−O) of ~60°. The only significant differences between the S_0 and T_1 geometry occur for the bond lengths within and between the thiophene rings. All C−S bond lengths increase by a few picometers in the T_1 state compared to the S_0 ground state (shown in Figure 10a and b for 2EDOT). For the C−C and C═C bonds of the thiophene rings, the changes in bond length reflect a transition of the ring from an aromatic to quinoid configuration in the T_1 state by a lengthening of the C═C and a contraction of the C−C bonds (Figure 10b). These changes are more pronounced for the smaller oligomers than for the longer ones. In the longer oligomers, the triplet state exciton is more easily accommodated and delocalized over more rings making geometry changes per ring smaller.

The harmonic frequency analysis of the singlet ground state of the OEDOTs in their DFT optimized geometries allowed determining the IR and Raman vibrational frequencies and intensities. The theoretical spectra are shown next to the experimental spectra for the high and low wavenumber regimes

(50) Louarn, G.; Buisson, J. P.; Lefrant, S.; Fichou, D. *J. Phys. Chem.* **1995**, *99*, 11399−11404.
(51) Hernández, V.; Casado, J.; Ramírez, F. J.; Alemany, L. J.; Hotta, S.; López Navarette, J. T. *J. Phys. Chem.* **1996**, *100*, 289−293.
(52) Hernández, V.; Casado, J.; Ramírez, F. J.; Zotti, G.; Hotta, S.; López Navarette, J. T. *J. Chem. Phys.* **1996**, *104*, 9271−9282.
(53) Casado, J.; Hotta, S.; Hernández, V.; López Navarette, J. T. *J. Phys. Chem.* **1999**, *103*, 816−822.
(54) Moreno Castro, C.; Ruiz Delgado, M. C.; Hernández, V.; Hotta, S.; Casado, J.; López Navarrete, J. T. *J. Chem. Phys.* **2002**, *116*, 10419−10427.
(55) Moreno Castro, C.; Ruiz Delgado, M. C.; Hernández, V.; Shirota, Y.; Casado, J.; López Navarrete, J. T. *J. Phys. Chem. B* **2002**, *106*, 7163−7170.
(56) Casado, J.; Hernández, V.; Ruiz Delgado, M. C.; Ortiz, R. P.; López Navarette, J. T.; Facchetti, A.; Marks. T. J. *J. Am. Chem. Soc.* **2005**, *127*, 13364−13372.
(57) Frisch, M. J., et al. *Gaussian* 03, revision B.04; 10; Gaussian, Inc.: Pittsburgh, PA, 2003.

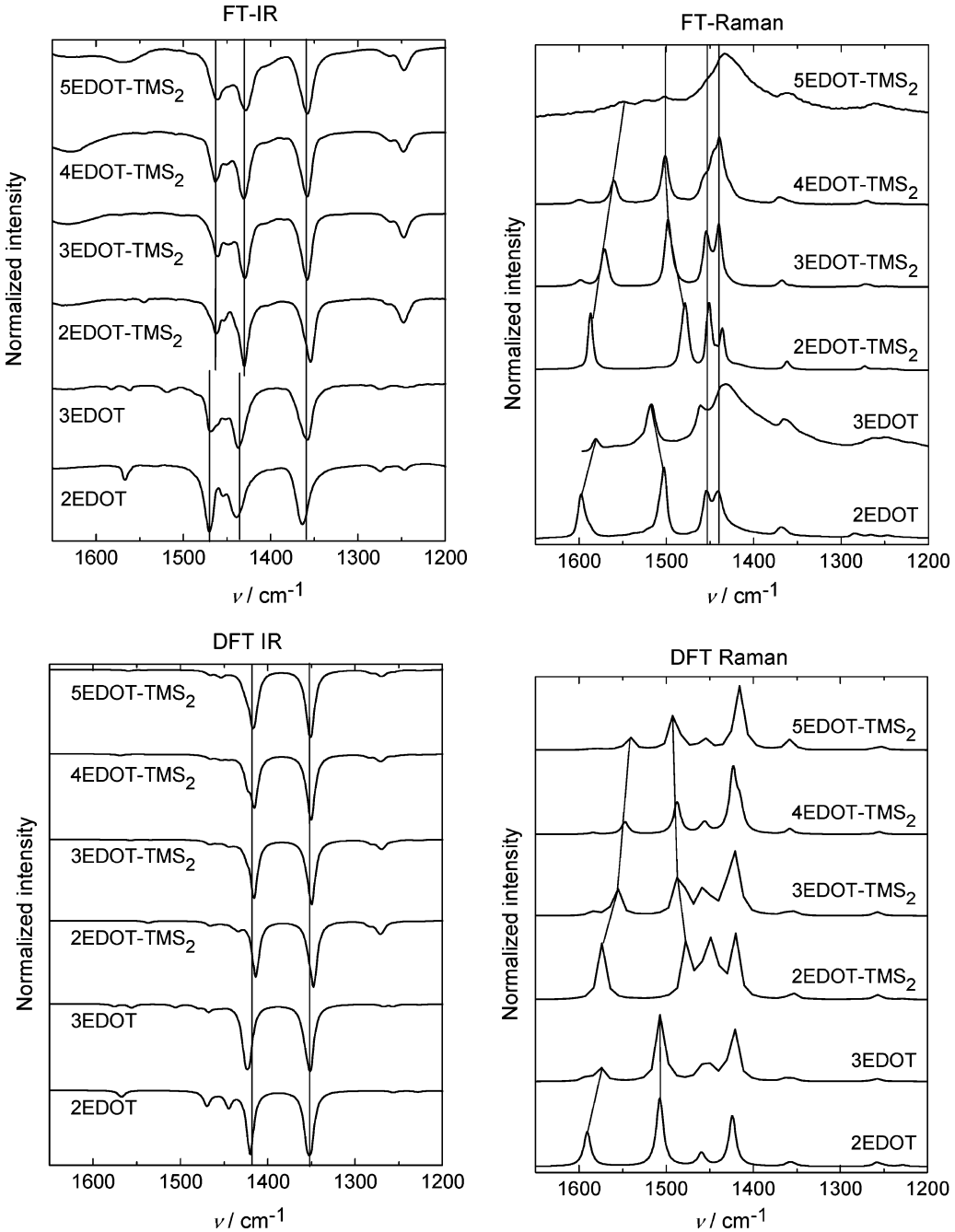

Figure 8. Experimental (FT) and theoretical (DFT) IR and Raman spectra of solid samples of OEDOTs at room temperature in the 1200−1700 cm^{-1} range. The wavenumbers in the DFT spectra have been corrected by multiplying by 0.96.[58]

in Figures 8 and 9, respectively, and reveal a good correspondence of the most salient features. The calculated wavenumbers were corrected by a factor of 0.96.[58]

The calculations can be used to assign the vibrational fine structure observed in the fluorescence spectra to specific modes. To appear in the electronic spectra, the coupling mode must be fully symmetric within the molecule's point group, assuming that the symmetry in the ground and excited state is the same. In an all-transoid conformation, the OEDOTs belong to the C_{2v} (for n odd) or the C_{2h} (for n even) point groups and vibrations must be of A_1 or A_g symmetry. As can be seen in the theoretical Raman spectra at least two bands with considerable intensity are present in the high-energy region (1400−1500 cm^{-1}). One of the bands that has the required A_1 or A_g symmetry is invariably found at 1422 ± 1 cm^{-1} for all OEDOTs. A second band (1476−1506 cm^{-1}) shows some dispersion with oligomer length. The vibrational frequencies of this last band are listed in Table 3 ($\tilde{\nu}_1$) for each of the oligomers and show generally good correspondence to the vibronic coupling in the fluorescence spectra. The DFT calculations identified this mode as being fully symmetric (A_1 or A_g) and involving mainly bond stretching modes in the thiophene rings. The overall mode represents a displacement of atoms along a coordinate that can be identified with the transformation of an aromatic structure into a quinoid structure, which is expected to couple strongly to the electronic transitions.

(58) Scott, A. P.; Radom, L. *J. Phys. Chem.* **1996**, *100*, 16502−16513.

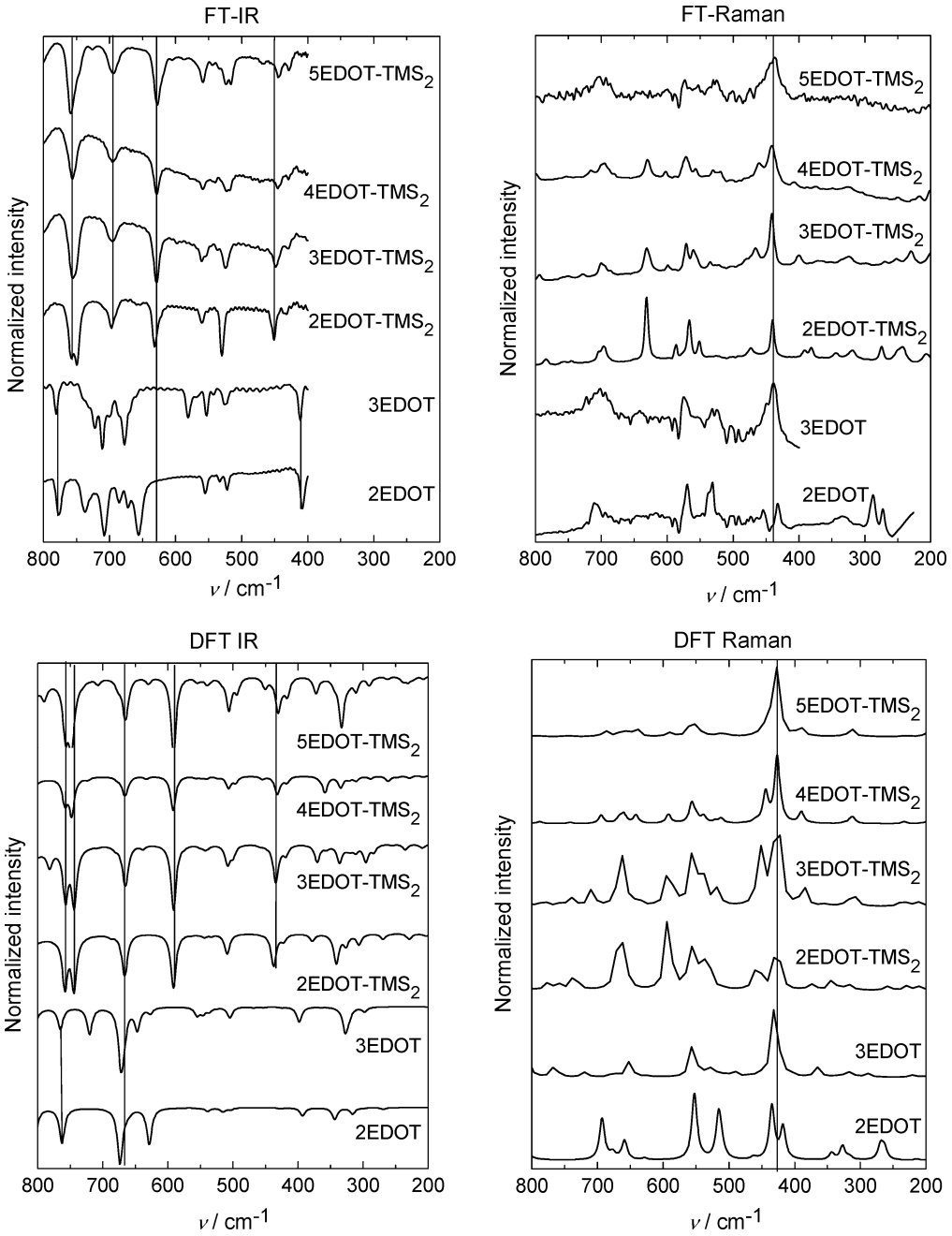

Figure 9. Experimental (FT) and theoretical (DFT) IR and Raman spectra of solid samples of OEDOTs at room temperature in the 200−800 cm^{-1} range. The wavenumbers of the DFT spectra have been corrected by multiplying by 0.96.[58]

For the low-energy vibration regime (400−500 cm^{-1}) a distinct band at 430 ± 5 cm^{-1} in the theoretical Raman spectra is associated with a fully symmetric (A_1 or A_g) mode. Its energy is similar to the low-energy vibronic spacing 440 ± 40 cm^{-1} observed in the fluorescence spectra. Based on this correspondence the second progression in the fluorescence spectra is assigned to be associated with this particular mode. The displacement vectors obtained from the DFT calculations show that for all OEDOTs this normal mode involves a deformation of the bond angles within the thiophene rings in a kind of breathing mode vibration and a change of the C−S bond lengths. This mode also affects the backbone of alternating double and single bonds of the conjugated oligomer because the changing bond angles influence the bond orders in the backbone. We conjecture that this causes the strong coupling to the electronic transition. There is another indication that points to this mode as being important to electronic excitations. The deformation caused by this mode resembles the deformation found when comparing singlet and triplet ground state geometries in, e.g., the 2EDOT (Figure 10b).

Energy and Geometry Relaxation in the Excited State. The intensity I_n of a transition between the vibrational ground state 0 in the initial electronic state and the *n*th vibrational level in the final electronic state is governed by the square of the Franck−Condon overlap

$$I_n = \langle v_0 | v_n \rangle^2 \tag{3}$$

with v as the vibrational wave function. In the harmonic

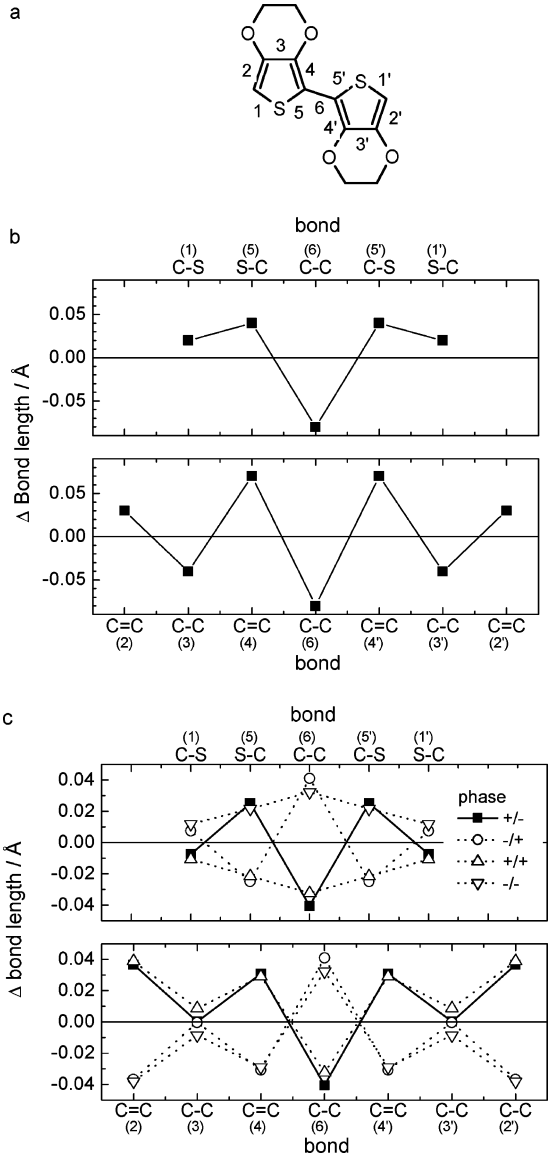

Figure 10. (a) Bond numbering of 2EDOT oligomer. (b) Change in bond length (Å) for 2EDOT between the S_0 and T_1 states along the sulfur atoms (top) and along the π-conjugated part (bottom) of the backbone from DFT geometry optimization. (c) Changes in bond length (Å) for for 2EDOT between the S_0 and S_1 states following the different phased combinations of the two normal modes Q_1 and Q_2 along the sulfur atoms (top) and the π-conjugated part (bottom) of the backbone using eq 9.

Table 3. Experimental Energy Spacing $\tilde{\nu}_1$ and $\tilde{\nu}_2$ from the Fluorescence Spectra and from DFT Raman Spectra Together with the Irreducible Representation of the Normal Mode $\Gamma(Q)$ in the Point Group of the Molecules

		fluorescence		DFT calculations			
compound	point group	$\tilde{\nu}_1$ (cm^{-1})	$\tilde{\nu}_2$ (cm^{-1})	$\tilde{\nu}_1$ (cm^{-1})	$\Gamma(Q_1)$	$\tilde{\nu}_2$ (cm^{-1})	$\Gamma(Q_2)$
2EDOT	C_{2h}	1490	480	1507	A_g	435	A_g
3EDOT	C_{2v}	1450	410	1506	A_1	431	A_1
2EDOT−TMS_2	C_{2h}	1480	460	1476	A_g	427	A_g
3EDOT−TMS_2	C_{2v}	1480	440	1484	A_1	427	A_1
4EDOT−TMS_2	C_{2h}	1450	430	1488	A_g	426	A_g
5EDOT−TMS_2	C_{2v}	1470	400	1490	A_1	426	A_1

approximation, the intensity can also be expressed in terms of the Huang−Rhys factor[59,60] S as a Poisson distribution $P_S(n)$ over the vibronic levels:

$$I_n = P_S(n) = \frac{e^{-S}S^n}{n!} \tag{4}$$

Within this formalism, the band shape of the low-temperature electronic spectra can be analyzed in more detail using eq 5, which simulates the spectrum as a sum over the Lorentzian-shaped vibrational peaks of both experimentally observed progressions.

$$I(E) = c\sum_m\sum_n \frac{\Gamma}{(E - E_{00} \mp m\tilde{\nu}_1 \mp n\tilde{\nu}_2)^2 + \Gamma^2}\left(\frac{I_m}{I_{m=0}}\right)\left(\frac{I_n}{I_{n=0}}\right) \tag{5}$$

In eq 5 the sums run over all peaks m and n of both progressions, Γ is the line broadening parameter, $\tilde{\nu}_1$and $\tilde{\nu}_2$ are the energies of the two vibrational modes, and $-$ or $+$ signs refer to absorption and emission spectra, respectively. I_m and I_n are determined by the Huang−Rhys parameters (S_1 and S_2) of the two modes according to

$$I_{mn} = I_m \times I_n = \frac{e^{-S_1}S_1^m}{m!}\frac{e^{-S_2}S_2^n}{n!} \tag{6}$$

Equation 5 has been used to determine the Huang−Rhys parameters S_1 and S_2 by adjusting $I(E)$ to the experimental spectra. Even for single values of Γ, $\tilde{\nu}_1$, and $\tilde{\nu}_2$, the simulated spectra follow the experimental spectra fairly well (see Supporting Information). The values for S_1 and S_2 resulting from the fits have been collected in Table 2 for each of the $S_1 \leftarrow S_0$, $S_1 \rightarrow S_0$, $T_1 \rightarrow S_0$, and $T_n \leftarrow T_1$ spectra.

Using the experimental Huang−Rhys parameters, information about the relaxation energy and the geometrical changes associated with an electronic transition can be obtained. The relaxation energy, E_{rel}, defined as the loss of vibrational energy in the final state after a vertical transition from the initial state, is directly related to the Huang−Rhys factor via

$$E_{rel} = S\tilde{\nu} \tag{7}$$

In addition, the Huang−Rhys parameter is related to the dimensionless displacement ΔQ of the minima of the potential energy curve along the normal coordinate Q upon electronic excitation according to[60]

$$S = \frac{(\Delta Q)^2}{2} \tag{8}$$

Since ΔQ is dimensionless, it gives a displacement relative to the zero-point motion that can be compared in different systems. Table 2 shows that the Huang−Rhys parameters associated with both modes decrease with increasing chain length for each of the different electronic transitions. For the longer oligomers the intensities of the transitions involving higher vibrational levels are suppressed compared to the 0−0 transition. This demonstrates that the vibrational relaxation energy associated with both modes decreases for longer oligomers. The trend that the maximum of the vibrational envelope shifts toward the 0−0 transition indicates that the electronic transitions cause less geometrical distortion in the larger

(59) Huang, K.; Rhys, A. *Proc. R. Soc. London Ser. A* **1950**, *204*, 406.
(60) Bässler, H.; Schweitzer, B. *Acc. Chem. Res.* **1999**, *32*, 173−182.

molecules than in shorter ones. This trend occurs for each of the $S_1 \leftarrow S_0$, $S_1 \rightarrow S_0$, $T_1 \rightarrow S_0$, and $T_n \leftarrow T_1$ transitions, albeit to a different degree and is interpreted in terms of a more extended delocalization of the excitation for the longer oligomers.

For the absorption ($S_1 \leftarrow S_0$) spectra, S_1 decreases from 0.92 for 2EDOT to 0.80 for 5EDOT−TMS_2, while S_2 is lowered from 0.72 to 0.30. This reveals that the low-energy vibrational mode become less frequently excited for longer oligomers. The experimental Huang−Rhys parameters for the fluorescence ($S_1 \rightarrow S_0$) spectra ($1.05 \geq S_1 \geq 0.68$ and $0.75 \geq S_2 \geq 0.32$) are very similar to those in the absorption, consistent with the fact that the same electronic states are involved. For the phosphorescence ($T_1 \rightarrow S_0$) spectra, both Huang−Rhys parameters for the 2EDOT oligomer ($S_1 = 1.12$; $S_2 = 1.03$) are much larger than those for the 3EDOT oligomer ($S_1 = 0.74$; $S_2 = 0.65$), with similarly large differences between 2EDOT−TMS_2 and 3EDOT−TMS_2. This indicates an appreciable excitation of both vibrational modes for the shorter oligomers and a larger displacement ΔQ between the T_1 and S_0 states. This experimental result is corroborated by the DFT calculations that reveal stronger geometry relaxation in the T_1 state for the shorter oligomers. Unfortunately, the low intensity of the phosphorescence spectra for the two longest oligomers precludes determining the corresponding Huang−Rhys factors from the spectra. It should be noted, however, that vibronic coupling in the triplet manifold along with spin−orbit coupling can introduce vibrationally induced intensities in the phosphorescence spectra, complicating this analysis.[61−64] Finally, in the $T_n \leftarrow T_1$ spectra, the Huang−Rhys parameter for the high-energy mode ($0.38 \geq S_1 \geq 0.20$) is much less than that for any of the other electronic transitions. The same result has been observed previously, e.g., in the $T_n \leftarrow T_1$ spectra of *p*-phenylene vinylene oligomers,[32] and seems to be a general property of π-conjugated oligomers. It signifies that the geometry relaxation for transitions between T_1 and the dipole-coupled T_n state are minimal.

The above analysis shows that the two modes exhibit rather similar trends with conjugation length and that the low-energy mode yields consistently smaller Huang−Rhys parameters than the high-energy mode. Hence, in the S_1 and T_1 states, larger distortions along the normal coordinate associated with the high-energy mode occur than for the low-energy mode and the distortions decrease with increasing chain length.

Geometry of the Singlet Excited State. By combining the normal vibrational modes known from the DFT calculations and the experimental Huang−Rhys parameters obtained by fitting eq 5, it is possible to determine the deformation of the molecule upon excitation from the S_0 ground state to the S_1 first singlet-excited state in a semiexperimental way.

Since the S_1 state is of interest here, the Huang−Rhys parameters associated with the absorption spectra (Table 2) are used. The exact (maximum) displacements during vibration along the normal coordinates are available from the DFT calculations and need only be converted to meaningful units, i.e., Å, by the equation

$$\Delta u_i = \sum_k \frac{l_{ik}\sqrt{2\hbar S_k}}{\sqrt{\omega_k \mu_k}} \tag{9}$$

where Δu_i (u runs over x, y, and z) denotes the displacement for each individual atom i in Å (for the exact procedure the reader is referred to the Supporting Information). The quantum chemical calculations provide for each normal mode k the individual normalized Cartesian displacements for all atoms in the x, y, and z directions (l_{ik}), the radial frequency ($\omega_k = 2\pi\tilde{\nu}_k c$), and the reduced mass μ_k.

For this analysis we limit the modes to the two fully symmetric modes Q_1 and Q_2 with energies $\tilde{\nu}_1$ and $\tilde{\nu}_2$ identified above and focus on 2EDOT as an example. To determine the geometry in the singlet excited state, the displacements along these two modes need to be taken into account simultaneously. Since it is not known if the displacements are toward greater or smaller values of Q_k for either mode, four different cases need to be considered. The first concerns the displacement toward greater values for both displacements ($+Q_1+Q_2$), while the other three are the corresponding permutations ($+Q_1-Q_2$, $-Q_1+Q_2$, and $-Q_1-Q_2$) in which one or two directions are reversed.

After determining the Cartesian displacements per atom in Å, the displaced bond lengths were determined and subtracted from the (nondisplaced) ground-state bond lengths, along the backbone, yielding the changes in bond length for the four situations (Figure 10c). Figure 10c applies to the first singlet excited state and can be compared to the changes in bond length calculated for the first triplet excited state in Figure 10. This comparison reveals that actually the $+Q_1-Q_2$ (■) combination of the two modes in the S_1 state provides a geometry change that resembles the T_1 state (Figure 10c). In this combination, the C═C double bonds elongate, the C−C single bonds are compressed, and the two C−S bonds closest to the center of the molecule elongate (Figure 10c). The other three combinations show less correspondence with Figure 10b. The maximum change in bond length in the S_1 state for this combination amounts to −4 pm for the central C−C bond which is of the same order of magnitude, but less than the value of −8 pm for the same bond of 2EDOT in the T_1 state derived from the DFT calculations. The larger geometry deformation of 2EDOT in the T_1 state than in the S_1 state inferred from this analysis is reflected in the fact that the Huang−Rhys parameters of both modes are larger in the phosphorescence spectra ($S_1 = 1.12$; $S_2 = 1.03$) indicating a stronger deformation than those in the fluorescence spectra ($S_1 = 1.05$; $S_2 = 0.75$), although the first may be affected by unknown contributions from vibronic coupling in the triplet manifold along with spin−orbit coupling to the intensity of the peaks in the vibrational progression.[61−64]

Conclusion

The photophyiscal properties of a series of OEDOTs with up to five repeat units have been studied using absorption, fluorescence, phosphorescence, and triplet-state absorption as well as IR and Raman spectroscopy. At low temperature in MeTHF, the OEDOTs undergo conformational relaxation to a more planar, well-defined structure. As a consequence, the inhomogeneous broadening in the optical spectra caused by the conformational disorder the OEDOTs is strongly reduced, and

(61) Albrecht, A. C. *J. Chem. Phys.* **1963**, *38*, 354−365.
(62) Lim, E. C.; Yu, J. M. H. *J. Chem. Phys.* **1967**, *47*, 3270−3275.
(63) Lim, E. C.; Yu, J. M. H. *J. Chem. Phys.* **1968**, *49*, 3878−3884.
(64) Griesser, H. J.; Bramley, R. *Chem. Phys.* **1982**, *67*, 373−389.

the spectra show an unprecedented highly resolved fine structure that can be associated with vibronic coupling to two different vibrational normal modes. The vibrational energies associated with the two vibrational progressions are very similar for each of the $S_1 \leftarrow S_0$, $S_1 \rightarrow S_0$, $T_1 \rightarrow S_0$, and $T_n \leftarrow T_1$ electronic transitions studied and amount to $\tilde{\nu}_1 = 180 \pm 20$ meV and $\tilde{\nu}_2 = 50 \pm 20$ meV, respectively. By comparing the vibronic coupling observed in the electronic spectra with experimental and theoretical DFT-based vibrational spectra, the coupling vibrations could be assigned to fully symmetric (A_1 and A_g) normal modes. The high-energy mode is associated with the well-known carbon−carbon bond stretch vibration that represents displacements analogous to the aromatic-to-quinoid deformation of rings and interring bonds. The low-energy mode involves a deformation of the bond angles within the thiophene rings and a change of C−S bond lengths.

The 0−0 bands of the $S_1 \leftarrow S_0$, $S_1 \rightarrow S_0$, $T_1 \rightarrow S_0$, and $T_n \leftarrow T_1$ transitions shift to lower energy with increasing length of the oligomer in a linear fashion with the inverse number of repeat units. The energy of the triplet state obtained from the phosphorescence spectra could be reproduced (subject to a systematic deviation of 0.12 eV) by quantum chemical DFT calculations starting from singlet geometry optimized structures. In the T_1 state, the optimized geometry of the OEDOTs shows changes in bond length compared to the optimized geometry in the S_0 state that point to an increased contribution of a quinoid structure. By analyzing the shape of the vibronic progressions in the spectra, the Huang−Rhys parameters S_1 and S_2 associated with the electronic transitions were obtained. It is found that S_2 is smaller than S_1 and that both S_1 and S_2 exhibit a downward trend with conjugation length. Hence in the S_1 and T_1 states, larger distortions along the normal coordinate associated with the high-energy mode occur than for the low-energy mode and the amount of distortion decreases with increasing chain length. For 2EDOT, the Huang−Rhys parameters determined from the experiment were combined with the normal modes from the DFT calculations to semiexperimentally predict the geometry in the S_1 state. The results indicate that the maximum changes in bond lengths in the S_1 state are less than those in the T_1 state, supporting a stronger geometry deformation in T_1 than in S_1.

In this study we have obtained a unique and detailed insight in the electronic structure and conjugation length dependence of the excited singlet and triplet states of ethylenedioxythiophene oligomers as model systems for PEDOT. The results may serve as an archetype for the excited-state behavior of other conjugated oligomers and polymers.

Acknowledgment. We would like to thank Dr. Bruce Anderson for his help in obtaining the FT Raman spectra. The research was supported by The Netherlands Organization for Scientific Research (NWO) through a grant in the PIONIER program.

Supporting Information Available: Time-resolved fluorescence traces of *n*EDOTs, fit of UV/vis spectrum of 3EDOT−TMS_2 to eq 5, Experimental Section, and complete ref 57. This material is available free of charge via the Internet at http://pubs.acs.org.

JA066920K